Chapter 2. Overview of the auroral substorm observation in 1989

2.1. Observations by the UV imager aboard the AKEBONO satellite in 1989

2.1.1 Instrumentation

The AKEBONO satellite was launched on February 22, 1989 into a semi-polar orbit with an initial apogee, perigee and inclination of, respectively, 10,500 km, 274 km and 75 deg and with an evolution period of 212 min [*Oya and Tsuruda*, 1990]. Hemispheric location of its apogee and perigee was reversed during about 9 months. The initial apogee was located in the southern hemisphere after the launch until middle of November in 1989. The AKEBONO is a spin-stabilized satellite, whose spin axis always directs to the sun, and its spin period is about 8 sec. The telemetry data from the AKEBONO in the southern hemisphere in 1989 were received and recorded at Syowa station in real time by the 30th Japanese Antarctic Research Expedition (JARE-30). JARE-30 also has constructed the receiving facility including the 11-m parabola antenna with a redome.

Two different kinds of auroral imagers were installed in the AKEBONO. One is for the auroral emission in visible wavelength from atomic oxygen (OI) green line (557.7 nm) (ATV-VIS), and the other is for the UV wavelength in the range of 115.0-139.0 nm (ATV-UV). The wavelength range of the ATV-UV is a range of the efficiencies more than 1 % of the peak value at about 123.0 nm. This wavelength range includes the nitrogen line at 120.0 nm, hydrogen Lyman-alpha at 121.6 nm, atomic oxygen lines at 130.4 and 135.6 nm, and the molecular nitrogen LBH (Lyman-Birge-Hopfield) bands. Specifications of the ATV-VIS and ATV-UV are described in detail by *Oguti et al.* [1990].

Instrumental block diagram of the ATV is shown in Figure 2.1. Center of the field-of-view (FOV) of the ATV always directs perpendicularly to the satellite spin axis. Auroral image captured by the ATV optics (OPT) is intensified by an image intensifier (II), and then focused on a CCD whose original pixel resolution is 488 x 376. Output from the CCD is amplified and then digitized by the 8 bit ADC (AD converter), and the digitized data are stored in a frame memory after a digital data compression process (DPCM). High voltage for the II, charge accumulation time of the CCD, gain of the amplifier, and DPCM on/off control are changeable by a programmable command sequence. High sensitivity of the ATV optical system enables us to obtain the auroral images in a short charge accumulation time of the CCD, less than 600 ms. Hence we can obtain a snapshot auroral image with a highest time resolution of the satellite spin period, about 8 seconds. To obtain a still image, a despun mirror system (DMS) is mounted in front of the ATV optics, which rotates the mirror reversely against the spin rotation with half of the spin angular velocity. The FOV of the ATV-VIS and ATV-UV are 30 deg x 40 deg and 36 deg x 36 deg, respectively. During the period around the apogee, observations by the ATV-VIS are very difficult because the bright sunlit area should be avoided from the FOV of the ATV-VIS. Hence during the period of the initial apogee in the southern hemisphere in 1989, only the ATV-UV data were available.

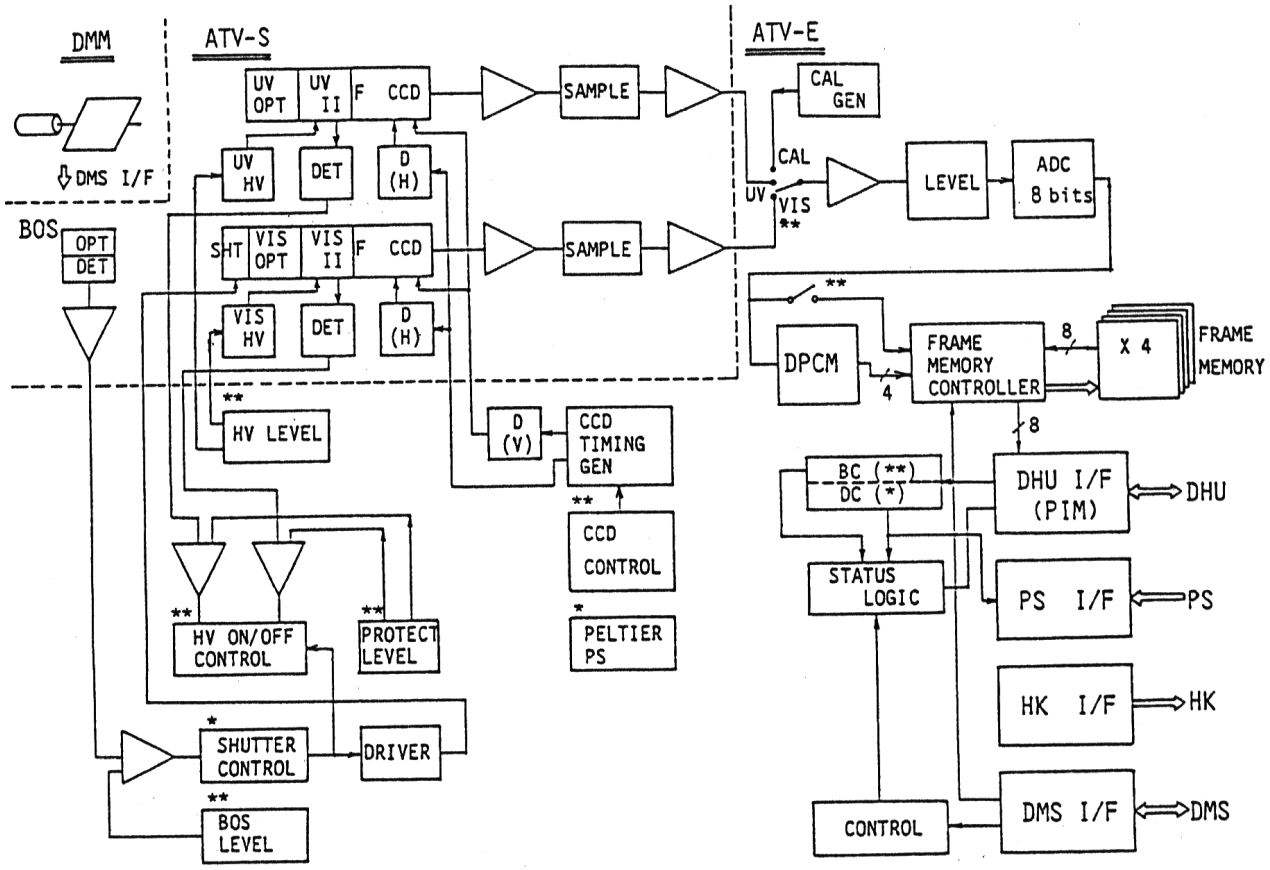

2.1.2 Auroral substorm evolution observed by the ATV-UV in 1989

Observations by the ATV-UV were carried out from April 12 until October 5 in 1989 in the southern hemisphere apogee orbit. We have checked all the images obtained in the total 459 satellite passes to find such an event where the auroral breakup occurs and the following evolution of the auroral bulge can be seen clearly. Total five such events were selected during the above period. Table 2.1 shows the date and time of the auroral breakup, the invariant latitude (ILAT0) and the magnetic local time (MLT0) of the central location of the initial brightening for the five events. All the events occurred in the premidnight hours. Such a premidnight preference of the onset region is consistent with previous works [e.g. *Elphinstone et al.*, 1995a]. Observations by the meridian scanning photometer (MSP) were carried out at Syowa station (SYO) during the period of the event 2, and at Asuka station (ASK) during the event 1 and 2. For the event 1, the auroral breakup occurred far eastward of ASK, and the azimuthal expansion of the auroral bulge did not reach the meridian of ASK. Hence the auroral poleward expansion was not observed by the MSP at ASK. During the event 2, the auroral breakup occurred at the close location westward of both ASK and SYO, and the auroral bulge expanded eastward beyond the meridians of the both stations. Hence, a clear poleward expansion was observed by the MSPs both at ASK and SYO. Furthermore, the IMF data from the IMP-8 satellite were also available during the event 2. From these and other aspects,

the event 2 is the most ideal and fortuitous event in 1989.

Table. 2.1. Auroral substorm events observed by the ATV-UV, which were selected from the total 459 pass during Apr. 12 to Oct. 5 in 1989.

event no	breakup date	breakup time (UT)	ILAT0 (deg)	MLT0 (hr)	MSP event	IMP-8 IMF
1	1989.6.05	20:40:07	68.3	23.1		○
2	1989.6.07	00:42:15	62.7	22.9	ASK SYO	○
3	1989.6.15	18:16:20	64.7	23.2		○
4	1989.8.10	14:24:17	62.9	23.0		
5	1989.8.15	12:24:22	64.5	20.8		○

Selected auroral images observed by the ATV-UV for each event are shown in Figure 2.2. All the images are projected on the ILAT vs MLT polar coordinates. Left and bottom of each panel are dusk and midnight, respectively. In the event 1, the auroral breakup occurred at relatively higher latitudes. The azimuthal expansion of the auroral bulge proceeded predominantly westward, and the eastward expansion did not reach the meridian of ASK. In the event 3, the auroral bulge became faint after it reached the ceiling latitude, and did not show further development around that local time. In contrast, the auroral oval on the western side of the bulge showed a significant poleward expansion after the bulge became faint. In the event 4, after the poleward expansion of the auroral bulge reached the ceiling latitude, the expansion proceeded mainly in the azimuthal direction. In the event 5, the breakup occurred at an earlier local time, and the auroral bulge showed a rapid evolution. In the last image, the poleward edge of the auroral region expanded around 80 deg ILAT, and the entire auroral region was separated into two regions, the discrete auroral region at the higher latitudes and the diffuse auroral region at lower latitudes. Such a configuration often appears during the period from the late expansion phase to the recovery phase of a well-developed substorm, and is called the "double oval" configuration [e.g. *Elphinstone et al.*, 1995b]. It should be noted that the breakup in the event 5 occurred around the time of the northward turning of the IMF. The auroral bulge evolution in the event 2 will be analyzed in detail in Chapter 3.

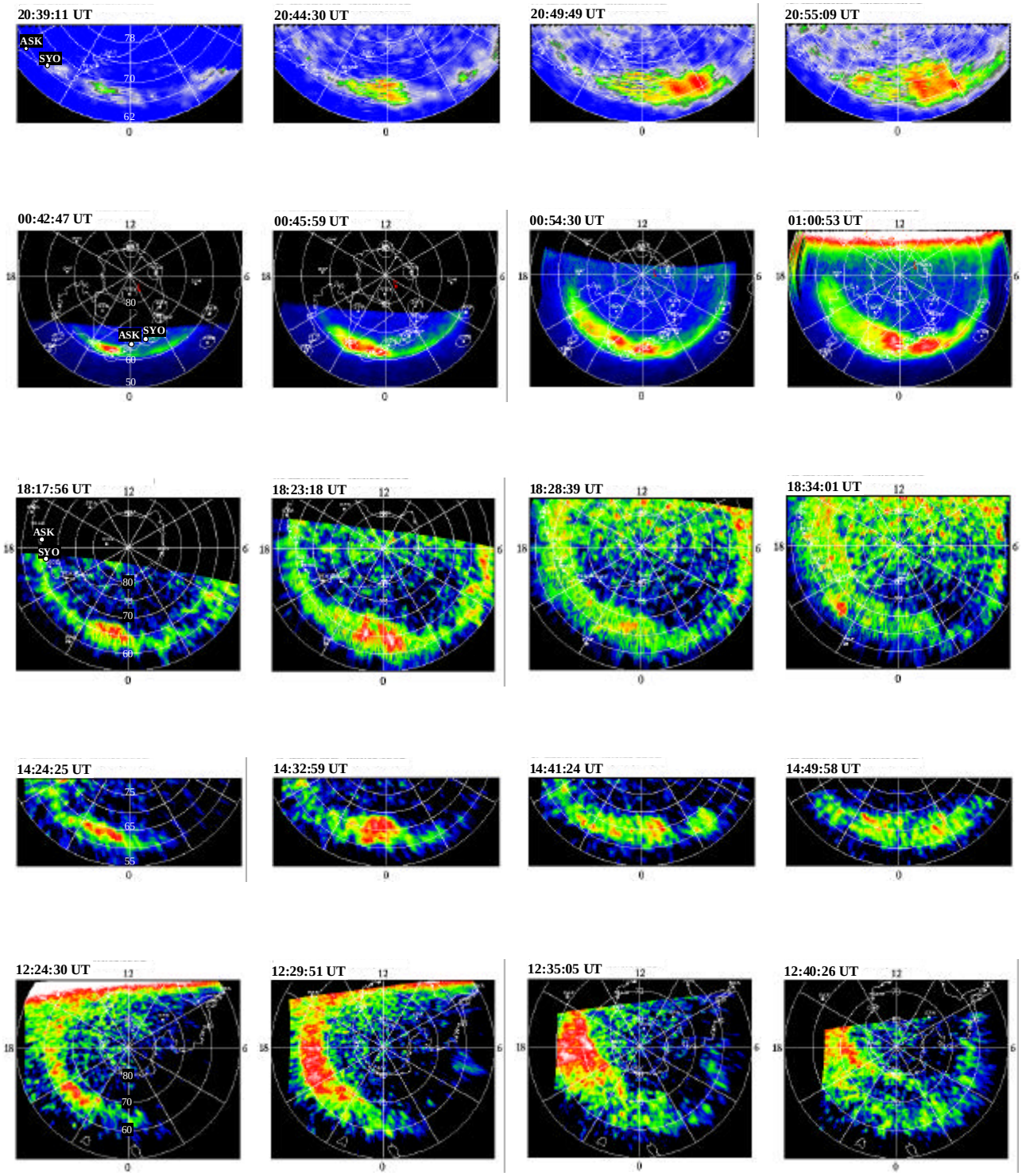

Figure 2.2. Selected auroral images observed by the ATV-UV for the 5 events listed in Table 2.1. Each image is projected on the ILAT vs MLT polar coordinates. Left and bottom of each panel are duskside and midnight, respectively.

2.2. Observations at Syowa and Asuka stations in 1989

2.2.1 Instrumentation

The optical instruments available at Syowa (SYO) (geographic latitude: -69.0 deg, longitude: 39.58 deg) and Asuka (ASK) (geographic latitude: -71.53 deg, longitude: 24.13 deg) stations in 1989 were the meridian scanning photometer (MSP) and the panchromatic all-sky SIT-TV camera at SYO, and the MSP at ASK, respectively. The Syowa MSP observed emissions from the atomic oxygen (OI) green line (557.7 nm) and red line (630.0 nm) and the hydrogen Balmer-line (486.1 nm (Hβ)) simultaneously. Its scanning speed was 180 deg/30 sec from horizon to horizon, and its FOV was 3 deg for the OI emissions and 5 deg for the Hβ emission. The tilting filter technique similar to *Fukunishi* [1975b] was adopted for the Hβ observation, and the tilting frequency was 1 Hz. The system block diagram of the MSP at SYO is shown in Figure 2.3. Output signals were digitized at 20 Hz, and the 1 Hz averaged data for the OI emissions and the intensity difference between the maximum and minimum outputs during the 1 sec tilting period for the Hβ emission are analyzed in this study. The effects of the air extinction and the van Rhijn are corrected. Specifications of the MSP at ASK were almost same as the MSP at SYO. The Asuka MSP observed one additional auroral emission from the N_2^+ first negative band (427.8 nm). Output signals are digitized and recorded by a digital data recorder at the sampling rate of 2 Hz. Original digitized values of the MSPs are transformed to the physical values in Rayleigh based on the calibration data obtained by a calibration lamp at each station. However, the absolute calibration of the calibration lamp itself has not yet been done. So we cannot discuss about the absolute intensity of each auroral emission, and only the relative variation of each emission will be discussed in this study.

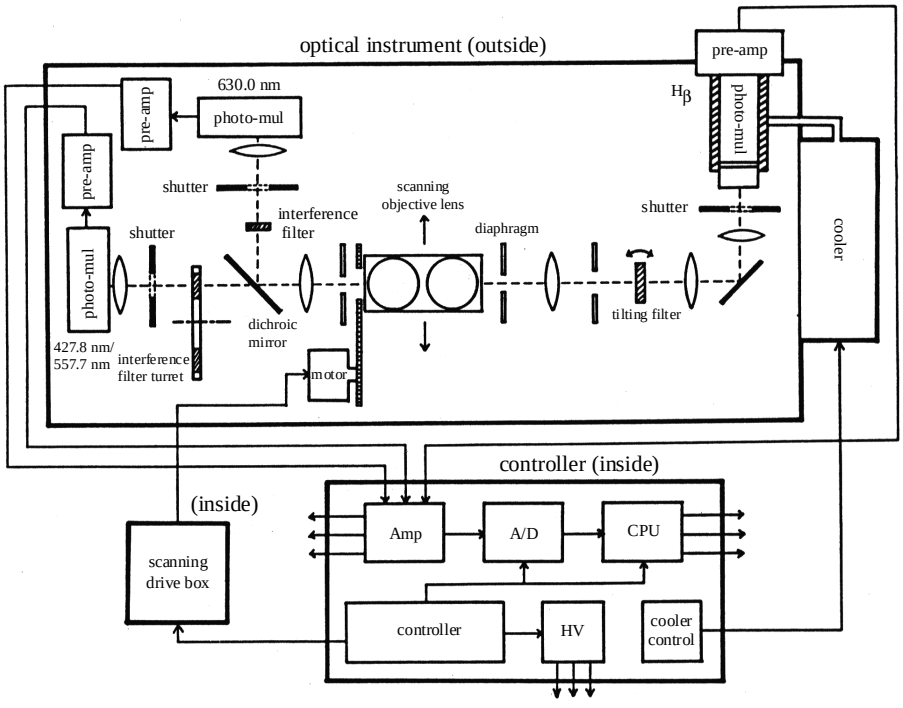

Figure 2.3. Block diagram of the MSP system at Syowa station in 1989.

We calculated the invariant latitude (ILAT) of the emission region from the observed scanning angle, assuming the emission altitude of 120 km for the 557.7 nm and Hβ emissions, and 250 km for the 630.0 nm emission. Figure 2.4 shows the relationship between the scanning angle and the ILAT both at SYO (Fig. 2.4(a)) and ASK (Fig. 2.4(b)). It can be seen in Fig 2.4 that the ILAT is almost linearly proportional to the scanning angle within the angle range above 30 deg elevation, and the relationship changes significantly outside of that range. The ILAT ranges for the 120 km and 250 km emissions at SYO are 58.89-75.67 deg and 56.35-80.26 deg, respectively, and those at ASK are 57.84-74.47 deg and 55.31-79.20 deg, respectively. Latitudinal resolutions within the range are 0.08-3.87 deg and 0.17-4.39 deg for the 120 km and 250 km emissions for the 1 Hz sampling at SYO, respectively, and those at ASK are 0.04-2.28 deg and 0.07-2.52 deg for the 2 Hz sampling, respectively.

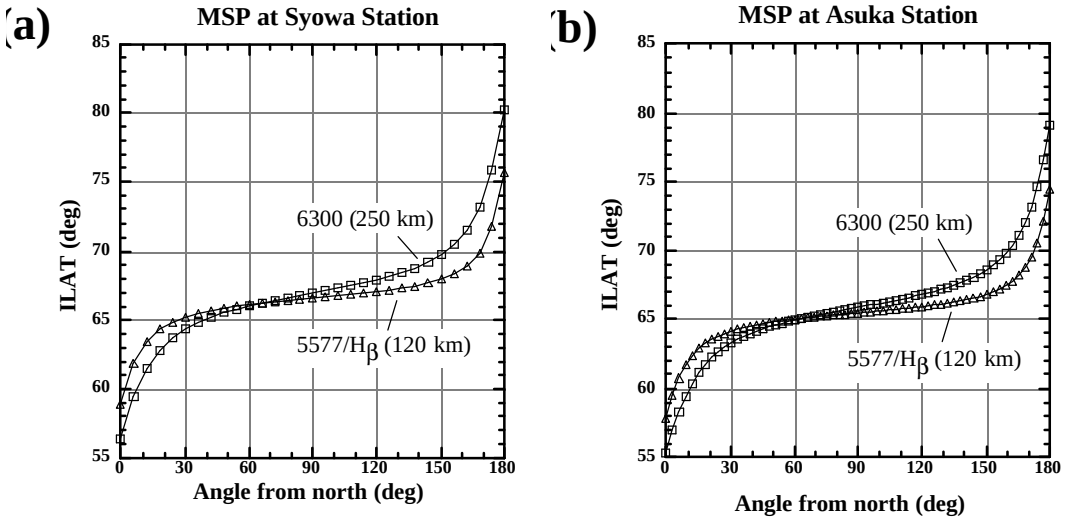

Figure 2.4. Relationship between the scanning angle and the ILAT of the MSP at both Syowa (a) and Asuka (b) stations. In each panel, square (triangle) symbol shows the relationship for the emission from 250 km (120 km) altitude.

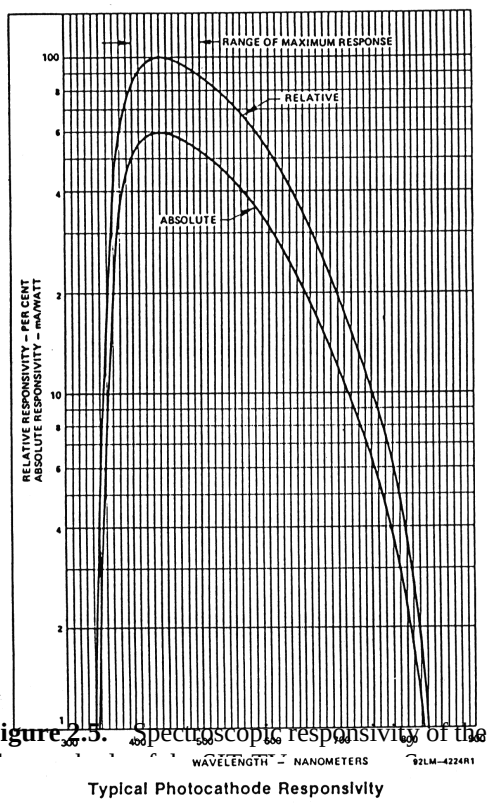

Figure 2.5. Spectroscopic responsivity of the

had a peak value around 427.8 nm as shown in Figure 2.5.
V camera, overlapped with the equi-elevation contours at 10
e available FOV of the SIT-TV camera was in the elevation
gnals from the SIT-TV camera were recorded by the video
30 Hz.

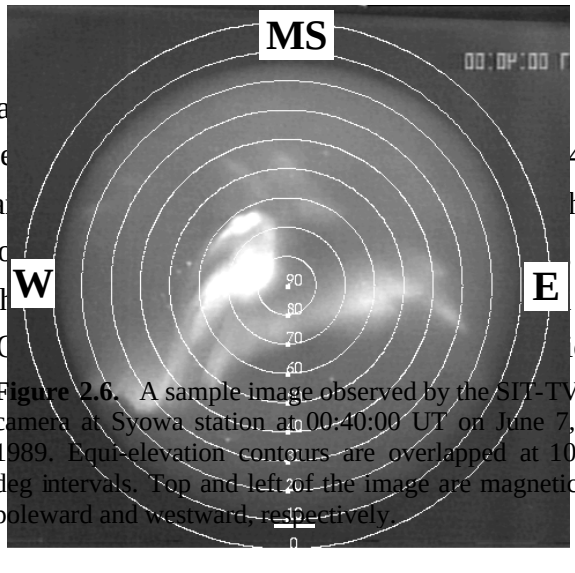

Figure 2.6. A sample image observed by the SIT-TV camera at Syowa station at 00:40:00 UT on June 7, 1989. Equi-elevation contours are overlapped at 10 deg intervals. Top and left of the image are magnetic poleward and westward, respectively.

ved at Syowa
ied out in the
nts from Ma
ard expansio
motion of th
data at SYO

of the latitude-time plot. The 16 nights were overlapped at both stations. The onset time (T0) of the significant poleward expansion was determined as the start time of the apparent poleward shift of the location of the maximum intensity in each auroral emission. The initial latitude (ILAT0) of the poleward shift was determined as the ILAT of the maximum intensity at the onset time.

Figure 2.7 sh ... by the MSP. The exa...es sh ... rved in the prem... e ... to morning hours, respective ... he TYPE-1, TYPE-2, and TY...

In the evolut ... he 557.7 nm and 630.0 nm em ... uroral oval, which is manife... he poleward expansion starts ... he electron auroral region. W ... o enhanced, which proceeds i... de side. The poleward expansi... xpansion is generally very high. Soon after the poleward expansion, the electron auroral region is often bifurcated into th ... part. As the lower la...le par ... intensified

(a)
TYPE-1

(b)
TYPE-2

(c)
TYPE-3

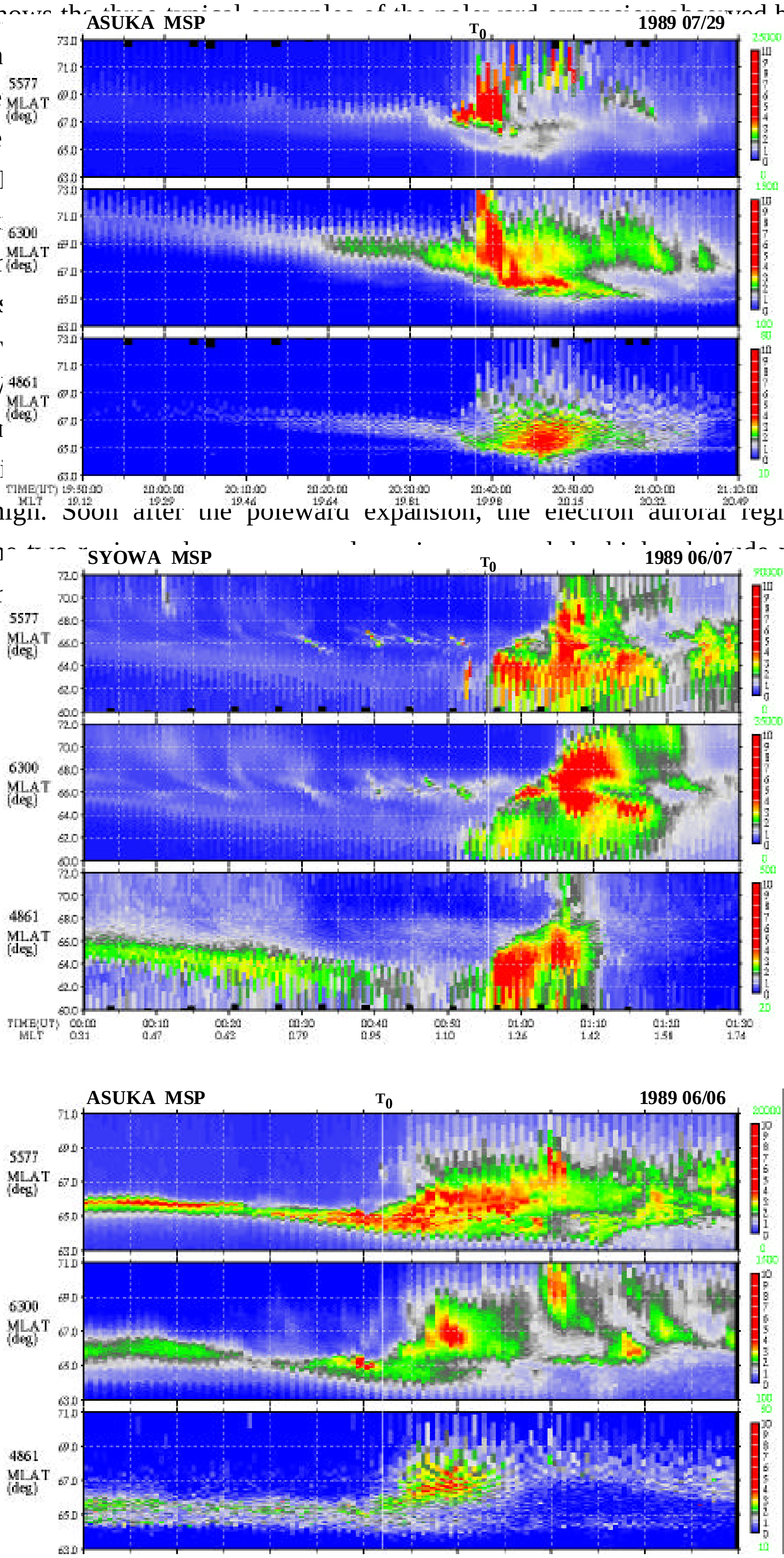

and expands equatorward first, and then the proton auroral emission gradually decreases from the lower latitudes.

In the evolution of the TYPE-2, the poleward expansion is characterized by the rapid poleward expansion of the both electron and proton auroral ovals. Within the initial rapid poleward expansion, both the electron and proton emissions co-exist and are intensified together. This initial poleward expansion is decelerated at some ceiling latitudes. After that time, an intense electron auroral activity often appears around the ceiling latitudes, around the poleward edge of the main oval. Sometimes the further poleward expansion starts with a significant intensification of the electron auroral activity around the poleward edge. Details of such type of the evolution will be described in Chapter 4.

In the evolution of the TYPE-3, the proton auroral oval is overlapped with the electron auroral oval, or the former is located at a little higher latitudes of the latter, before the poleward expansion starts. The poleward expansion starts with the intensification of both the electron and proton emissions in the middle of the both auroral ovals. The speed of the poleward expansion is relatively low. Soon after the poleward expansion starts, the proton auroral region gradually shifts its location poleward, or the proton auroral emission becomes weak from the lower latitudes.

Similar kind of the difference in the poleward expansion in the different local time sector was also described by *Vallance Jones et al.* [1982]. They followed the auroral evolution observed by the meridian scanning photometers at 10 min intervals, which seems too coarse to follow the detailed evolution as shown in Fig. 2.7.

A summary of the total 88 events is shown in Table 2.2. The occurrence number of the TYPE-1, -2, and -3 was 41, 32, and 15, respectively. Average start location of the initial poleward expansion in each type is also shown in Table 2.2. The MLT0 is the average magnetic local time of the station at T0, and the ILAT0 is the average values of the ILAT at T0. It can be seen that the TYPE-1 (TYPE-3) occurred in the most pre-midnight (post-midnight) hours, and the TYPE-2 occurred around the midnight hours, as expected. The initial poleward expansion started at higher latitudes in the case of the TYPE-1 and TYPE-3, compared with the TYPE-2.

Table. 2.2. A summary of poleward expansion events observed by MSP in 1989.

expansion type	events	MLT0 (hour)	ILAT0 (deg)
TYPE-1	41	21.8	66.1
TYPE-2	32	23.5	63.0
TYPE-3	15	25.0	65.2
TOTAL	88	23.0	64.8

Figure 2.8 shows the distribution of the start location of the initial poleward expansion for the total 88 events. Cross, triangle, and circle symbols in Fig. 2.8 indicate the expansion type of the TYPE-1, -2, and -3, respectively. Two equatorward borders of the statistical auroral oval by *Feldstein and Starkov* [1967] are also shown for the two cases of the magnetic activity index of Q=1 (quiet time) and Q=6 (disturbed time). Although the distribution is rather scattered, it seems that the start locations are nearly aligned the distribution of the statistical auroral oval.

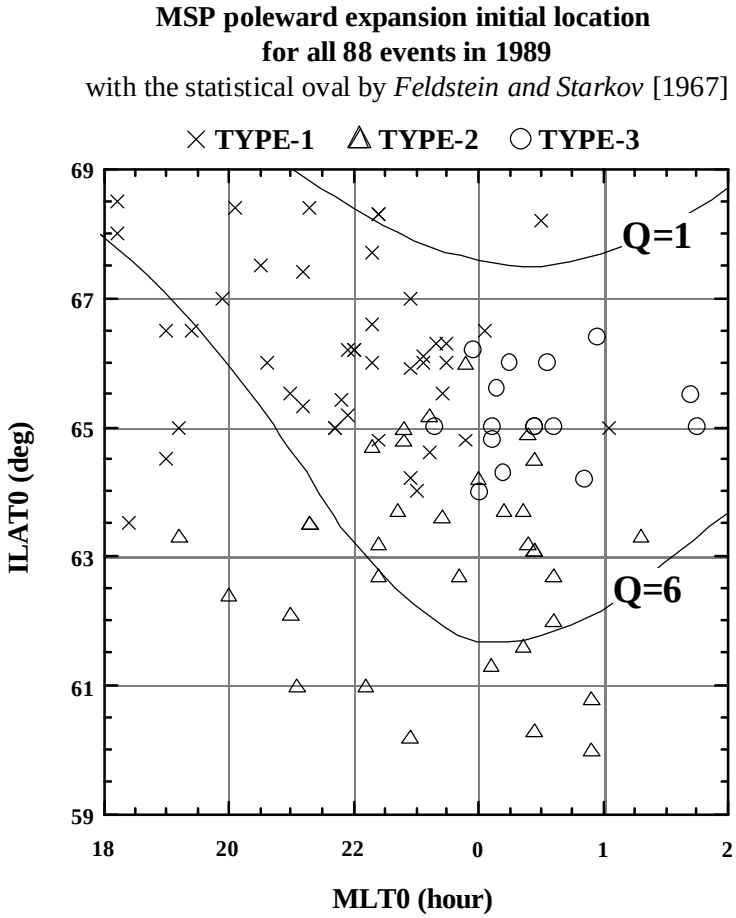

Figure 2.8. Distribution of the start location of the initial poleward expansion observed by the MSP for the total 88 events in 1989. Cross, triangle, and circle symbols correspond to the expansion type of the TYPE-1, -2, and -3, respectively. Two equatorward borders of the statistical auroral oval by *Feldstein and Starkov* [1967] are also shown for the two cases of the magnetic activity index of Q=1 (quiet time) and Q=6 (disturbed time).